



Higher Order Mode Measurement and Analysis in 1.3 GHz and 3.9 GHz Superconducting Accelerating Cavities at FLASH and the European-XFEL

Cristina Martin Perez (Complutense University Madrid)

Han Niu (TsingHua University, Beijing)

Supervisors:

Nicoleta Baboi (DESY)

Liangliang Shi (DESY / University of Manchester)

DESY Summer Student Programme 2015

September 8, 2015

Abstract

An electron beam entering an accelerating superconducting cavity excites a wakefield. This wakefield can be decomposed into a series of Higher Order Modes (HOMs), resonant electromagnetic fields that oscillate in the cavities with frequencies higher than the accelerating frequency. HOMs carry information about the beam and the cavity and can be used for beam diagnostics. This report summarizes the HOM measurements and analysis in the TESLA 9-cell 1.3 GHz Superconducting Cavities at FLASH and in the Third Harmonic 3.9 GHz Superconducting Cavities at the European-XFEL. It presents the measured spectra of such cavities and analyses the stability and quality factors of the corresponding HOMs.

Contents

1	Introduction	3
1.1	FLASH	3
1.2	E-XFEL	4
1.3	The TESLA 9-cell Superconducting Cavities	5
1.4	The Third Harmonic Superconducting Cavities	6
2	Motivation	7
3	Theory	8
3.1	Particle Acceleration	8
3.2	Wakefields	9
3.3	Higher Order Mode Characteristics	9
3.4	S-Parameters	10
4	Beam Measurements in TESLA 9-cell Superconducting Cavities at FLASH	11
4.1	HOM Measurements with RSA	11
4.2	HOM Characterization	13
4.3	HOM Stability over Time	14
4.4	Quality Factors	19
4.5	HOM Dependence on the RF Power Applied	22
5	S-parameter Measurements in Third Harmonic Cavities for the E-XFEL	26
5.1	Measurement of S_{21} Parameter with NWA	26
5.2	Transmission Spectra and HOM Characterization for Single Cavities at Room Temperature	27
5.3	Transmission Spectra and HOM Characterization for a Single Cold Cavity	31
6	Conclusions	36
7	Appendix: 3.9 GHz Cavities	38

1 Introduction

Charged particles accelerated in a superconducting cavity induce electromagnetic fields. As these particles move through the cavity the geometry of the structure changes, so the induced wall currents can not keep up with the bunch. Part of the electromagnetic fields remain behind and reflections occur. These electromagnetic fields generated by the beam itself interacting with the environment are known as wakefields. Such wakefields act back on the following particles causing bunch instabilities. The consequence is normally an enlargement of the energy distribution and an increase in the transverse emittance.

On the other hand, wakefields carry information about the beam and the cavity and can be used to do beam diagnostics: wakefield signals can serve as beam position and beam phase monitors.

Wakefields can be decomposed into so-called Higher Order Modes (HOM), resonant electromagnetic fields with frequency higher than the accelerating frequency. Two types of HOMs are the monopole and the dipole modes: monopoles have azimuthal symmetry in the transverse plane, while dipoles present two nodes azimuthally. In multicell cavities, these modes can be grouped in passbands, frequency ranges where a number of modes are densely spaced.

This report studies HOMs in two accelerating structures at two facilities: the TESLA 9-cell Superconducting Cavity at FLASH (DESY) and the Third Harmonic Superconducting Cavities at the European-XFEL (E-XFEL) (Hamburg).

- For the TESLA 9-cell Superconducting Cavity at FLASH, the study focuses on the analysis of the stability of two HOM bands: (a) the 2nd monopole passband ($\sim 2.4 \text{ GHz}$), that could be used for beam phase monitoring inside the cavity, and (b) the 1st dipole passband ($\sim 1.7 \text{ GHz}$), that could be used for beam position monitoring.
- For the Third Harmonic Superconducting Cavity at the E-XFEL, the study focuses on the spectra analysis of (a) the 1st and 2nd dipole passbands ($4.0 - 5.6 \text{ GHz}$) and (b) the 5th dipole passband ($9.0 - 9.1 \text{ GHz}$), which can be used for beam position monitoring.

1.1 FLASH

FLASH[9] (Free-electron LASer in Hamburg) is DESY's free-electron laser user facility providing ultra-short femtosecond laser pulses in the EUV and soft X-ray wavelength range with unprecedented brilliance. FLASH is a high-gain free-electron laser (FEL) which achieves laser amplification and saturation within a single pass of a bunch of electrons through a long undulator. The lasing process is initiated by the spontaneous undulator radiation. The FEL works then in the so-called Self-Amplified Spontaneous Emission (SASE) mode without needing an external input signal. FLASH is also a pilot facility for the E-XFEL project and a test bed for further research and development for linear collider related superconducting accelerator technologies. A schematic overview of the FLASH facility is shown in Figure 1.

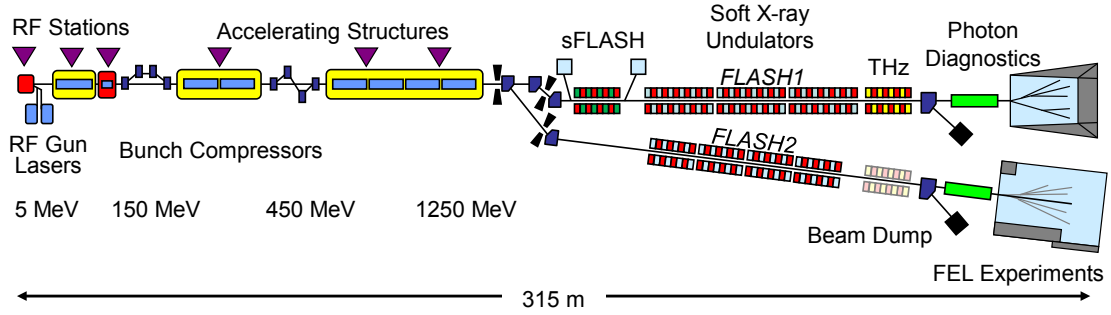


Figure 1: Schematic overview of FLASH (not to scale). Beam direction is from left to right, the total length is 315 m. Both beamlines are shown, the old FLASH1 beamline and the new FLASH2 beamline.

The electron beam generated by a photoelectric gun is accelerated off-crest by eight superconducting TESLA cavities in cryomodule ACC1. The fundamental mode of operation is the 1.3 GHz mode, which is used to accelerate the beam. To linearize the energy spread of the bunch, harmonics of the fundamental accelerating frequency of the main linac are added by third harmonic superconducting cavities operating at 3.9 GHz in the ACC39 module.

Some parameters for the FLASH facility are shown in Table 1:

Maximum electron energy	1250 <i>MeV</i>
Peak current	2.5 <i>kA</i>
Emittance	2 <i>mmrad</i>
Pulse repetition frequency	10 <i>Hz</i>
Shortest SASE wavelength	4.2 <i>nm</i>

Table 1: FLASH parameters 2015.

1.2 E-XFEL

The E-XFEL[10] (European X-Ray Free-Electron Laser) is a research X-ray laser facility currently under construction which is scheduled to start user operation in 2017. The 3.4 km long tunnel housing the superconducting linear accelerator and photon beam lines will run 6 to 38 m underground, from the site of the DESY research center in Hamburg to the town of Schenefeld in Schleswig-Holstein.

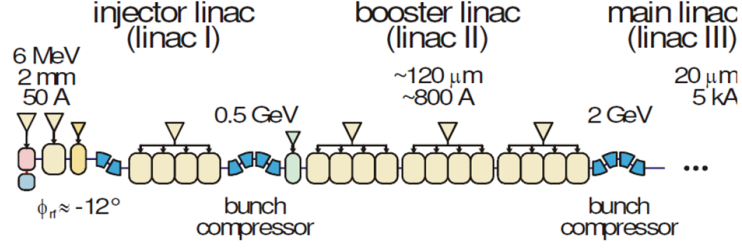


Figure 2: Schematic the E-XFEL injector. Beam direction is from left to right.

The electrons will be accelerated to an energy of up to 17.5 GeV by a 2.1 km long superconducting linear accelerator containing TESLA cavities. In order to generate the high quality electron beam required for the short wavelength FEL operation, the injector part includes a third harmonic (3.9 GHz) accelerating module, similar to FLASH. Like at FLASH, the bunches are introduced into the magnetic field of special arrays of magnets called undulators, where they follow curved trajectories resulting in the emission of X-ray radiation. This is increasingly amplified until an extremely short and intense X-ray flash is finally created, with properties similar to those of laser light.

Some parameters for the E-XFEL facility are shown in Table 2:

Maximum electron energy	17.5 <i>GeV</i>
Peak current	5 <i>kA</i>
Emittance	0.4 – 1.0 <i>mmrad</i>
Pulse repetition frequency	10 <i>Hz</i>
Shortest SASE wavelength	0.05 <i>nm</i>

Table 2: E-XFEL parameters.

The E-XFEL will be widely applied in many fields of scientific research and industry. For example, it can be used to make non-destructive stereo imaging for live cells, direct observation of the life processes in the cells. It can also be used to study a variety of rapid changes in state, nano-scale materials science research, etc.

1.3 The TESLA 9-cell Superconducting Cavities

The TESLA 9-cell superconducting cavity (Figures 3 and 4) is a standing wave 9-cell 1m-long structure made of niobium. The fundamental mode is a π -mode, which means that the direction of the electric field alternates from cell to cell, with a frequency of 1.3 *GHz*. It is designed to achieve an accelerating gradient larger than 25 *MV/m* and a quality factor above 5×10^9 .

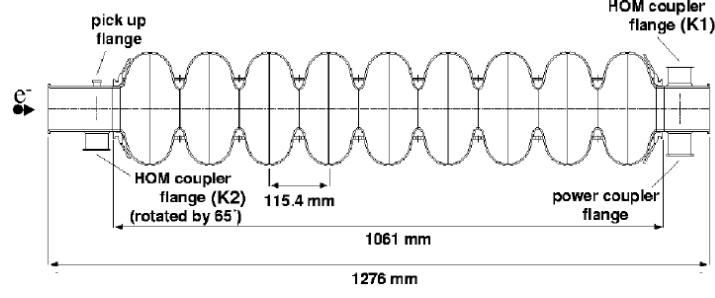


Figure 3: Design of the TESLA accelerating cavity. The cavity is positioned in the module such that the beam comes from the left.

The shape of the cells was optimized in order to avoid high local fields. The end half-cells have a slightly different shape in order to ensure the field flatness in all cells. The power coupler is placed downstream.

One HOM coupler is mounted on the beam tube at either side. They reduce the effect of the HOMs by extracting their stored energy. They are almost perpendicular to each other in order to ensure damping of both polarizations of the dipole modes.

1.4 The Third Harmonic Superconducting Cavities

The third harmonic superconducting cavity (Figure 4) is a standing wave 9-cell 0.35 m-long structure made of niobium, similar to the TESLA cavity. The fundamental mode is a π -mode, with a frequency of 3.9 GHz.

The third harmonic cavities will linearize the bunch RF curvature distortions and minimize beam tails in the bunch compressor[6]. They are installed in the injector part of FLASH, where there are 4 cavities, and the E-XFEL, where there are 8 cavities (Figure 5).

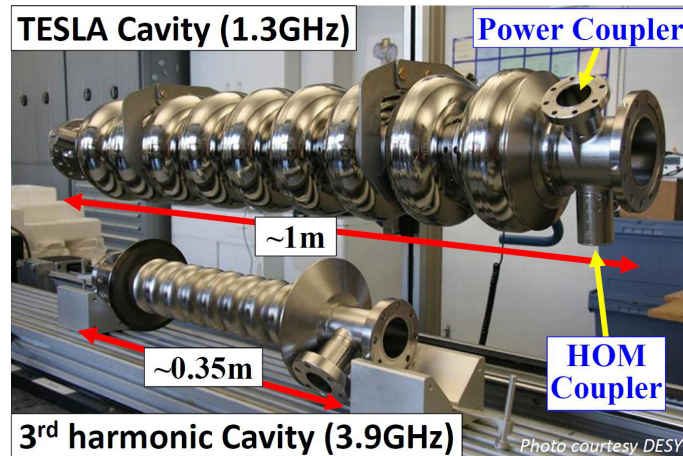


Figure 4: 1.3 GHz and 3.9 GHz cavities



Figure 5: E-XFEL 3rd harmonic accelerating module

By design, the 3.9 GHz cavity has two features in terms of wakefields, compared to the 1.3 GHz cavity. First, the wakefields in the 3.9 GHz cavity are larger than those in the 1.3 GHz cavity as the iris radius is significantly smaller: 15 mm in the 3.9 GHz cavity compared to 35 mm in the 1.3 GHz cavity. Second, the HOM spectrum is significantly more complex than that of the 1.3 GHz cavity. The main reason for this is that, unlike the TESLA cavity case, the majority of the modes are above the cutoff frequencies of the beam pipes. This allows most of the modes from each independent cavity to propagate through to adjacent cavities[8]. Therefore, most modes reach all HOM couplers.

2 Motivation

Wakefields can be decomposed in the so-called Higher Order modes (HOM), resonant electromagnetic fields that oscillate with a frequency higher than the accelerating frequency. HOMs carry information about the beam (position, phase, charge, etc.) and the cavity (imperfection, axis, etc.). Therefore, HOMs can be used to do beam diagnostics from the energy radiated to the HOM couplers. On one hand, one can do beam phase monitoring based on monopole signals of the TESLA 9-cell 1.3 GHz superconducting cavities. On the other hand, one can do beam position monitoring based on dipole signals of the TESLA 1.3 GHz and the third harmonic 3.9 GHz superconducting cavities.

In order to monitor the beam phase and position at the 1.3 GHz cavities, one needs stable frequencies. In this report, the stability over time of the 2nd monopole passband and the 1st dipole passband for the TESLA cavities, as well as the quality factors of the corresponding modes, has been studied. The influence of the RF power applied to the cavities on the HOMs has also been measured.

In view of monitoring the beam position at the 3.9 GHz cavities, the characterization of their spectrum has to be done. This has been done for the 1st, 2nd and 5th dipole passbands of the third harmonic superconducting cavities for the E-XFEL. The frequencies of the measured HOMs have been compared to simulations and the quality factors have been calculated.

The work is also relevant for future electron-positron linear colliders, considered to be an essential instrument for future experiments in particle physics. An important parameter of a collider is the luminosity, the collision rate of the particles. In order to obtain a high luminosity, the emittance of the beam, a measure of the distribution of transverse

positions and angles of the particles, has to be very small. There, the study of the behavior of wakefields is important since they are the main source of emittance increase for ultra-relativistic bunches.

3 Theory

3.1 Particle Acceleration

The accelerating structures used nowadays are RF structures. A single metallic cylindrical cavity, called pillbox, can be used to accelerate a charged beam. For such a cavity one can calculate analytically the resonant electromagnetic fields, or modes.

The various modes differ in frequency and field distribution inside the cavity. They can be classified into transverse magnetic (TM) and transverse electric (TE) modes. TM modes have no longitudinal magnetic field on the axis ($B_z = 0$), while TE modes have no longitudinal electric field ($E_z = 0$), therefore not being appropriate for acceleration.

When many pillboxes are coupled together, each mode degenerates into as many coupled modes as the number of cells forming a band of modes. The field lines are distorted, and the modes are no longer purely TE or TM.

Consider any mode in a cavity with the frequency $f = \omega/(2\pi)$. One obtains in complex notation for the electric and magnetic field in cylindrical coordinates (r, ϕ, z) :

$$\mathbf{E}(r, \phi, z, t) = \mathbf{E}_0(r, \phi, z) \exp(-i\omega t) \quad (1)$$

$$\mathbf{B}(r, \phi, z, t) = \mathbf{B}_0(r, \phi, z) \exp(-i\omega t) \quad (2)$$

Generally the fields $\mathbf{E}_0(r, \phi, z)$ and $\mathbf{B}_0(r, \phi, z)$ in geometries with cylindrical symmetry can be written as (in a multi-pole expansion):

$$\mathbf{E}_0(r, \phi, z) = \sum_m (E_{0r}^{(m)}(r, z) \cos(m\phi) \mathbf{e}_r + E_{0\phi}^{(m)}(r, z) \sin(m\phi) \mathbf{e}_\phi + E_{0z}^{(m)}(r, z) \cos(m\phi) \mathbf{e}_z) \quad (3)$$

$$\mathbf{B}_0(r, \phi, z) = \sum_m (B_{0r}^{(m)}(r, z) \sin(m\phi) \mathbf{e}_r + B_{0\phi}^{(m)}(r, z) \cos(m\phi) \mathbf{e}_\phi + B_{0z}^{(m)}(r, z) \sin(m\phi) \mathbf{e}_z) \quad (4)$$

According to the azimuthal field distribution of the modes, there are monopole modes ($m = 0$), with azimuthal symmetry, dipole modes ($m = 1$), when there are two nodes of the field amplitude azimuthally, as well as quadrupole, sextupole etc. modes. Normally, monopole modes are dominant among the modes with longitudinal electric field, while dipole modes dominate the modes with transverse field. Figure 6 shows an example of the azimuthal distribution of the electric field of a monopole and a dipole modes.

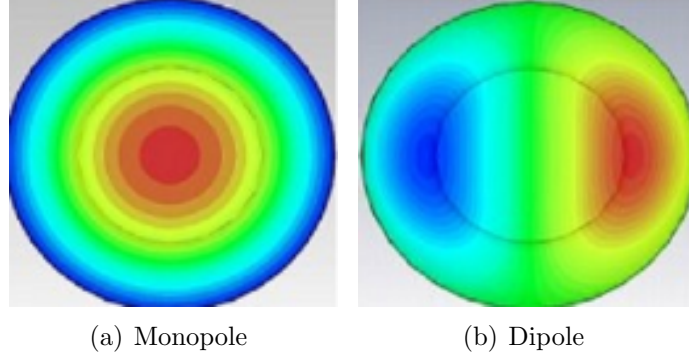


Figure 6: Examples of monopole and dipole transverse electric fields.

3.2 Wakefields

When a charged particle travels through a perfectly conducting cylindrical pipe, as is approximately the case in an accelerator, the electromagnetic field lines move together with the particle. This is illustrated in Figure 7(left) for the case of a bunch with Gaussian charge distribution. When the geometry of the walls changes, the wall currents can not keep up with the bunch (middle). A part of the electromagnetic field generated by the charge remains behind. When the beam enters the tube again, reflections of the field may occur (right). This constitutes the so-called wakefields. Another charge following the first one interacts with these fields, leading to a change in its energy or orbit.

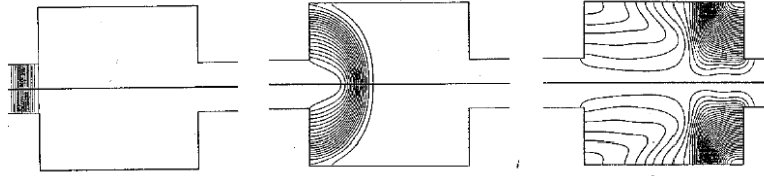


Figure 7: Wakefield generation when a Gaussian bunch passes a change in geometry in the vacuum pipe. Three moments in time are shown. [5].

The long range wakefields, meaning those that affect the following bunches, can be written as a sum of Higher Order Modes (HOM) that oscillate in the cavities. These modes can be grouped in passbands, frequency ranges where a number of modes are densely spaced.

3.3 Higher Order Mode Characteristics

We need to use some characters like frequency, Q factor, dissipation factor, to describe a higher order mode. Usually, there will be damping in the sinusoidally driven resonators and the energy in the resonance system will continue to decrease. Nevertheless, at some resonant frequencies the damping is small and the oscillation will last longer than usual.

One can use the quality factor (Q) to determine the qualitative behavior of simple damped oscillators. Q is the ratio of the energy stored in the oscillating resonator to the energy dissipated per cycle by damping processes:

$$Q = \frac{\omega E}{P} \quad (5)$$

where E is the stored energy and P is the power dissipated. We can see from the equation above that a high Q means that the energy is stored in the resonator for a long time.

Q can be calculated by the frequency-to-bandwidth ratio of the resonator:

$$Q = \frac{f_0}{B} \quad (6)$$

$$B = f_2 - f_1 \quad (7)$$

where f_0 is the resonant frequency and B is the half-power bandwidth.

In the resonant cavities we are studying here, the fundamental frequency used to accelerate the electrons are 1.3 GHz and 3.9 GHz. Nonetheless, as we have seen, the cavity also has many HOMs above these frequencies. Especially in superconducting cavities, where the HOMs have a high Q , the resonant energy will be stored for a long time. When the next bunch passes, the energy does not decrease but rather adds up. HOM couplers are used to extract energy from the cavity, and thus decrease the Q .

3.4 S-Parameters

For a microwave system, a field analysis method should be used, but this method is too complicated. Therefore, often a simplified method of analysis is needed: the microwave network analysis.

The S-parameter is an important parameter in the microwave transmission. It describes the electrical behavior of linear electrical networks when undergoing various steady state stimuli by electrical signals.



Figure 8: Two-port network.

The S-parameter matrix for the 2-port network (see Figure 8) is probably the most commonly used and serves as the basic building block for generating the higher order matrices for larger networks. In this case the relationship between the reflected and incident power waves is given by the following S-parameter matrix:

$$\begin{pmatrix} b_1 \\ b_2 \end{pmatrix} = \begin{pmatrix} S_{11} & S_{12} \\ S_{21} & S_{22} \end{pmatrix} \begin{pmatrix} a_1 \\ a_2 \end{pmatrix} \quad (8)$$

Therefore, each 2-port S-parameter has the following generic descriptions:

- S_{11} : input port voltage reflection coefficient
- S_{12} : reverse voltage gain
- S_{21} : forward voltage gain
- S_{22} : output port voltage reflection coefficient

The complex linear gain is $G = S_{21}$, that is simply the voltage gain as a linear ratio of the output voltage divided by the input voltage, all values expressed as complex quantities. This is the parameter that will be measured in the E-XFEL 3rd harmonic cavities.

4 Beam Measurements in TESLA 9-cell Superconducting Cavities at FLASH

Experimental studies of the HOM properties of the superconducting 9-cell TESLA cavities working at 1.3 GHz were performed. This report focuses on the study of the following modes:

- TM monopole modes in the 2nd passband (~ 2.4 GHz).
- TE dipole modes in the 1st passband (~ 1.7 GHz).

Several measurements of these modes have been conducted over periods of time. The idea is to prove the stability of the HOMs in time. Moreover, the influence of the power applied to the cavity on these modes has been studied.

4.1 HOM Measurements with RSA

Wakefields were excited with bunched electron beams in FLASH (see Figure 9). HOMs were detected from HOM Coupler 1 of the first cavity in module 6 (ACC6). The signal is passed to the Tektronix RSA (Real-time Spectrum Analyzer), that records real-time spectra. The data was imported and analysed with MATLAB[11] with the Instrument Control Toolbox.

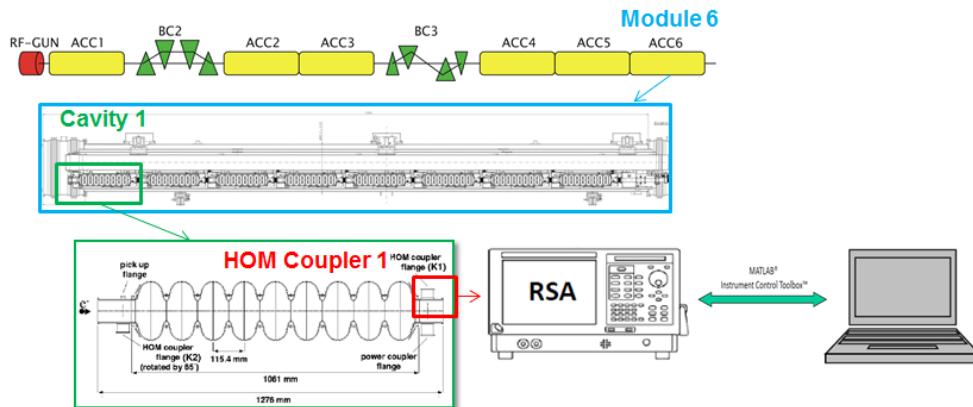


Figure 9: Experimental setup of the measurements. The beam enters module 6 (ACC6) from left to right. Measurements of HOM are taken with RSA from the HOM Coupler 1 in Cavity 1 and analyzed in the computer with MATLAB.

Figure 10 shows an example of a spectrum with 4 modes in the second monopole passband and Figure 11 shows an example of a mode in the 1st dipole passband. The x-axis is the frequency f while the y-axis shows the intensity of the signal in dBm.

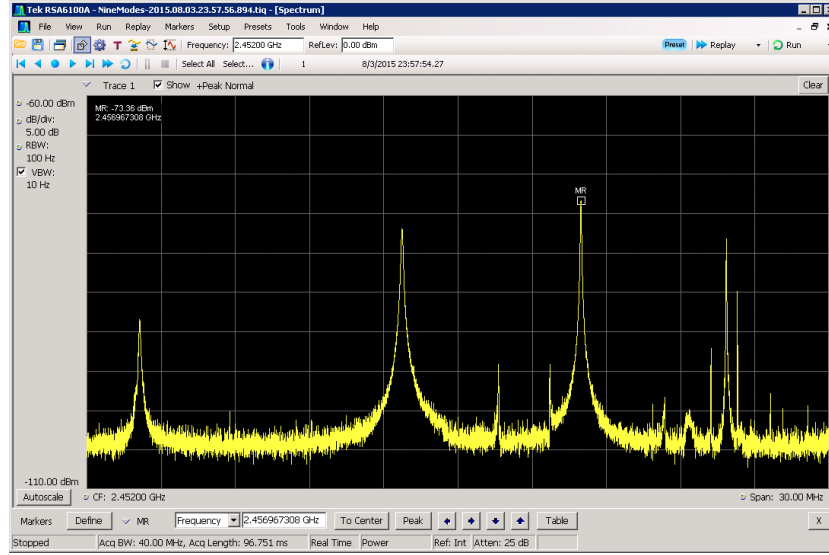


Figure 10: Modes in the 2nd monopole passband as measured with the Real-time Spectrum Analyzer. The study will be focused on the most intense 4 peaks.

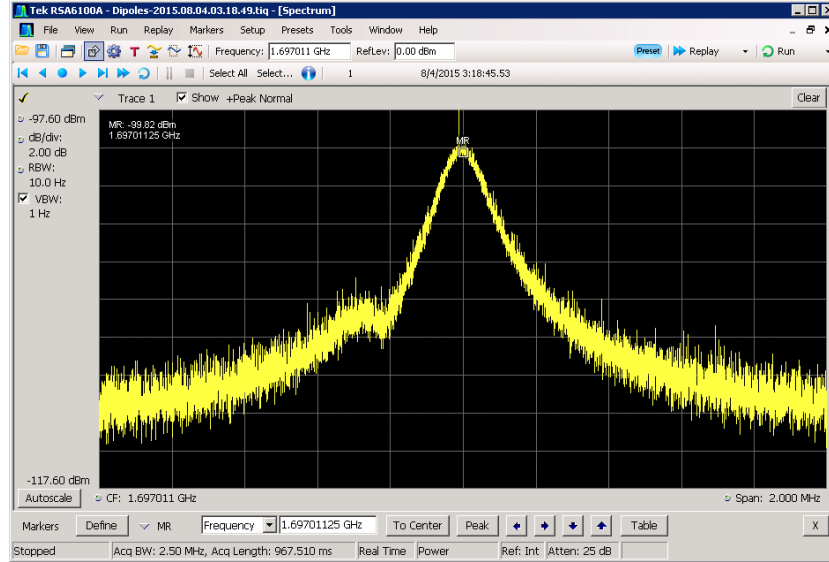


Figure 11: Mode in the 1st dipole passband as measured with the Real-time Spectrum Analyzer. One can notice two peaks very close together as a result of the polarization of the dipole.

4.2 HOM Characterization

The peak frequencies of the aforementioned modes were measured from RSA and recorded. Nonetheless, this method may bring some systematic errors due to the noise present in the spectra. Therefore, HOMs were also identified using a global Lorentzian fit technique. The mathematical expression of the fit summed over all the peaks in the spectrum is:

$$y = \sum_i \frac{a_{i_0}}{1 + \left(\frac{x - a_{i_1}}{a_{i_2}} \right)^2} \quad (9)$$

where i is the mode index, a_{i_0} the amplitude, a_{i_1} the center and a_{i_2} the Full Width at Half Maximum (FWHM).

The quality factor for each mode i can be obtained from the fit:

$$Q_i = \frac{a_{i_1}}{a_{i_2}} \quad (10)$$

The software PeakFit[12] has been used for the fits. Figure 12 shows the fit results of the 2nd monopole passband shown in Figure 10, while Figure 13 shows the fit results of the 1st dipole passband shown in Figure 11. The goodness of fit was measured by the coefficient of determination r^2 , a number that indicates how well the data fit a statistical model, expressed as the square of the sample correlation coefficient (i.e., r) between the outcomes and their predicted values. In this context, $r^2 = 1$ is a perfect fit and $r^2 = 0$ is a poor fit. Fits with coefficients of determination below $r^2 = 0.95$ were dismissed in our study.

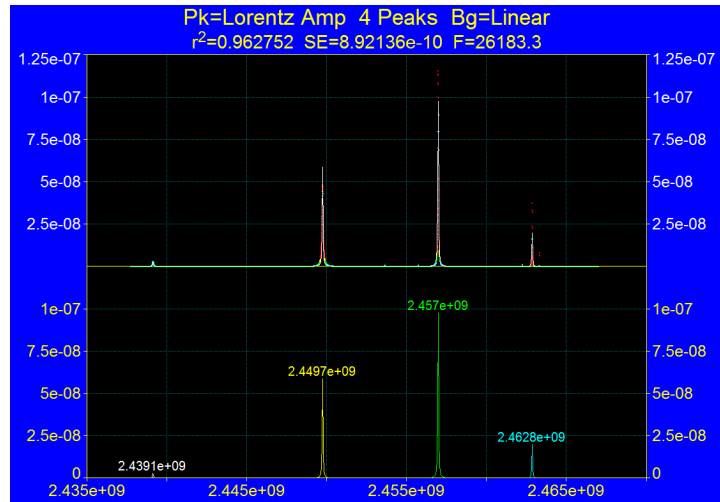


Figure 12: Lorentzian fit of the 2nd monopole passband in Figure 10: up: measured; down: the outcome of the fit. The numbers show the peak center frequencies. The coefficient of determination r^2 is shown above the plots.

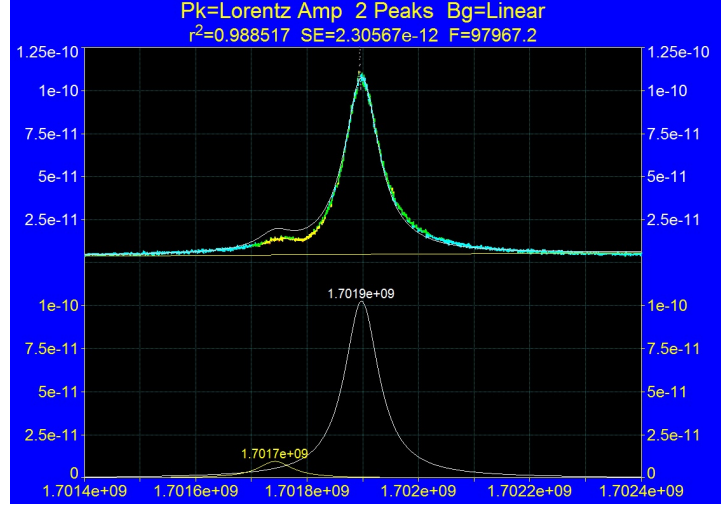


Figure 13: Lorentzian fit of the 1st dipole passband in Figure 11: up: measured; down: the outcome of the fit. The numbers show the peak center frequencies. The coefficient of determination r^2 is shown above the plots.

4.3 HOM Stability over Time

The results of the peak characterization for the 2nd monopole passband, both from RSA and from the Lorentzian fit with PeakFit, for different dates and times of measurement, are shown in Table 3 and Figure 14:

Table 3: Measured (RSA) and fitted (PeakFit) frequencies of the 4 peaks in the 2nd monopole passband for different dates and times.

Date / Time	Frequency Peak 1 (MHz)		Frequency Peak 2 (MHz)	
	RSA	PeakFit	RSA	PeakFit
2015.08.03 / 22:59:09	2439.1346	2439.1338	2449.7356	2449.7356
2015.08.03 / 23:57:56	2439.1346	2439.1331	2449.7356	2449.7369
2015.08.04 / 00:38:20	2439.1375	2439.1339	2449.7385	2449.7369
2015.08.04 / 00:40:49	2439.1288	2439.1339	2449.7385	2449.7371
2015.08.04 / 01:44:49	2439.1346	2439.1331	2449.7385	2449.7370
2015.08.04 / 01:46:21	2439.1317	2439.1309	2449.7356	2449.7368
2015.08.04 / 01:47:09	2439.1375	2439.1353	2449.7327	2449.7369
2015.08.04 / 02:12:31	2439.1288	2439.1342	2449.7385	2449.7371
2015.08.04 / 02:12:49	2439.1317	2439.1341	2449.7384	2449.7368
2015.08.04 / 02:34:51	2439.1231	2439.1324	2449.7385	2449.7367
2015.08.04 / 02:38:02	2439.1375	2439.1341	2449.7356	2449.7371
2015.08.04 / 02:40:52	2439.1260	2439.1317	2449.7356	2449.7379
2015.08.04 / 03:10:32	2439.1317	2439.1332	2449.7355	2449.7372
2015.08.04 / 03:11:35	2439.1317	2439.1337	2449.7356	2449.7369
2015.08.04 / 03:12:02	2439.1346	2439.1336	2449.7356	2449.7371
2015.08.04 / 03:12:42	2439.1288	2439.1336	2449.7356	2449.7371
2015.08.04 / 03:29:15	2439.1346	2439.1338	2449.7356	2449.7368
2015.08.20 / 02:33:28	2439.1317	2439.0798	2449.7385	2449.7356
2015.08.20 / 02:34:17	2439.1260	2439.0827	2449.7384	2449.7356

Date / Time	Frequency Peak 3 (MHz)		Frequency Peak 4 (MHz)	
	RSA	PeakFit	RSA	PeakFit
2015.08.03 / 22:59:09	2456.9673	2456.9673	2462.8462	2462.8447
2015.08.03 / 23:57:56	2456.9644	2456.9673	2462.8433	2462.8446
2015.08.04 / 00:38:20	2456.9673	2456.9673	2462.8433	2462.8446
2015.08.04 / 00:40:49	2456.9644	2456.9673	2462.8462	2462.8445
2015.08.04 / 01:44:49	2456.9673	2456.9674	2462.8462	2462.8449
2015.08.04 / 01:46:21	2456.9673	2456.7897	2462.8462	2462.8449
2015.08.04 / 01:47:09	2456.9673	2456.9674	2462.8433	2462.8447
2015.08.04 / 02:12:31	2456.9702	2456.9026	2462.8433	2462.8446
2015.08.04 / 02:12:49	2456.9673	2456.9671	2462.8433	2462.8447
2015.08.04 / 02:34:51	2456.9673	2456.9673	2462.8433	2462.8446
2015.08.04 / 02:38:02	2456.9673	2456.9673	2462.8462	2462.8448
2015.08.04 / 02:40:52	2456.9702	2456.9673	2462.8462	2462.8447
2015.08.04 / 03:10:32	2456.9673	2456.9673	2462.8433	2462.8446
2015.08.04 / 03:11:35	2456.9673	2456.9672	2462.8462	2462.8446
2015.08.04 / 03:12:02	2456.9673	2456.9673	2462.8433	2462.8454
2015.08.04 / 03:12:42	2456.9673	2456.9673	2462.8433	2462.8447
2015.08.04 / 03:29:15	2456.9673	2456.9673	2462.8462	2462.8447
2015.08.20 / 02:33:28	2456.9673	2456.9673	2462.8462	2462.8462
2015.08.20 / 02:34:17	2456.9673	2456.9673	2462.8462	2462.8453

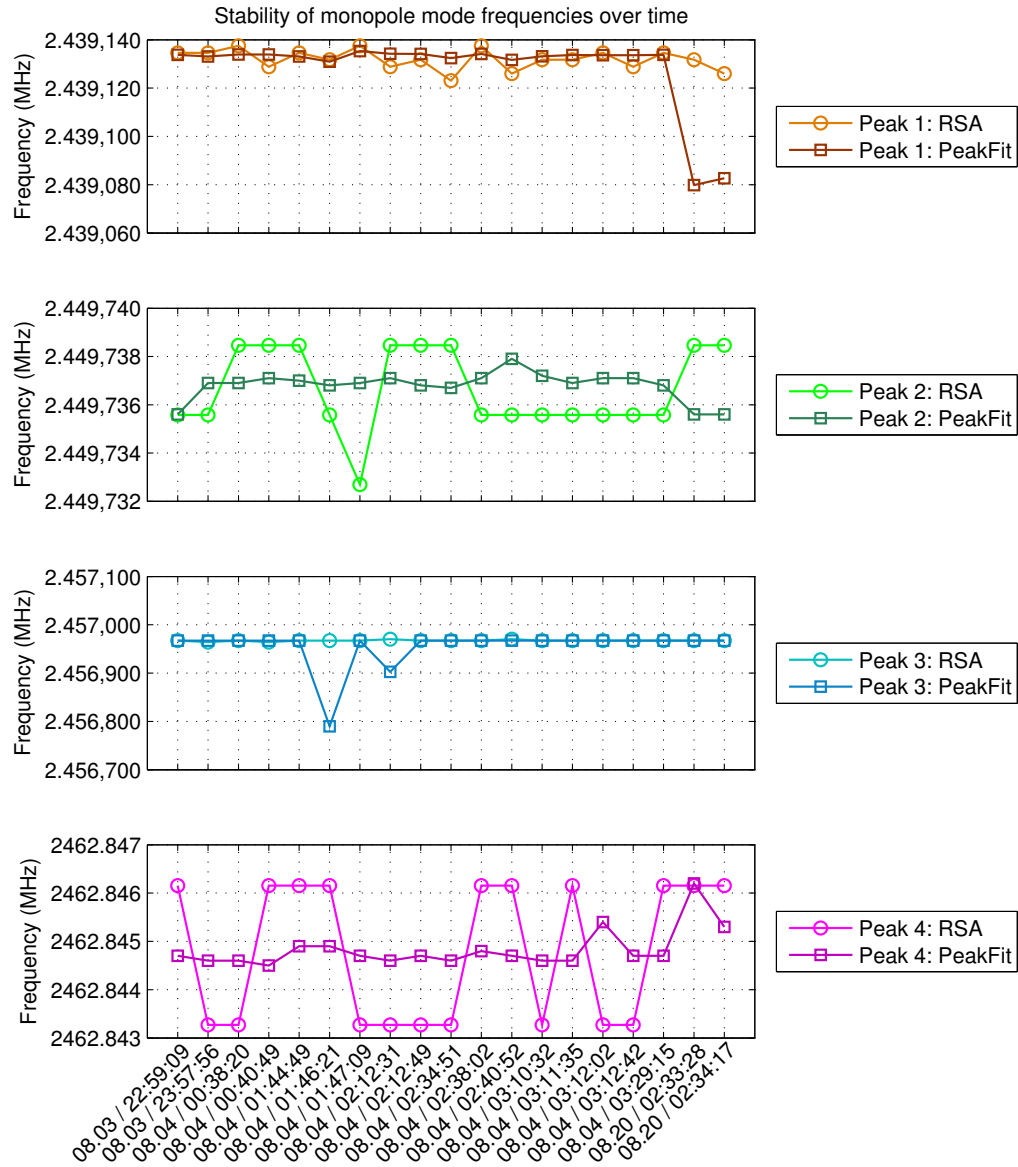


Figure 14: Measured (RSA) and fitted (PeakFit) frequencies of the 4 peaks in the 2nd monopole passband for different dates and times.

The variations of each peak in time are shown in Table 4:

Table 4: Mean frequencies, standard deviation and relative error of the 4 peaks in the 2nd monopole passband for different dates and times.

Peak	Average frequency (MHz)	Standard deviation (MHz)	Relative error
1	2439.1279	0.0165	0.0007%
2	2449.7368	0.0006	0.00002%
3	2456.9545	0.0426	0.002%
4	2462.8448	0.0004	0.00002%

One can conclude that the monopole modes of the 2nd passband remain constant over time.

The results of the peak identifications in the 1st dipole passband, both from RSA and after the Lorentzian fit with PeakFit, for different dates and times of measurement, are shown in Table 5 and Figure 15:

Table 5: Measured (RSA) and fitted (PeakFit) frequencies of the 2 peaks in the 1st dipole passband for different dates and times.

Date / Time	Frequency Peak 1 (MHz)		Frequency Peak 2 (MHz)	
	RSA	PeakFit	RSA	PeakFit
2015.04.22 / 10:17:58	1701.6900	1701.9008	1702.1453	1702.1238
2015.04.22 / 10:18:12	1701.7000	1701.9011	1702.1340	1702.1225
2015.04.22 / 10:18:19	1701.7050	1701.9015	1702.1557	1702.1235
2015.04.22 / 10:20:50	1701.7125	1701.7020	1702.1363	1702.1460
2015.04.22 / 10:20:54	1701.7005	1701.7008	1702.1281	1702.1458
2015.04.22 / 10:20:59	1701.7193	1701.7016	1702.1494	1702.1460
2015.04.22 / 10:21:03	1701.7190	1701.7016	1702.1433	1702.1460
2015.04.22 / 10:21:07	1701.7084	1701.7026	1702.1356	1702.1457
2015.05.01 / 23:03:41	1696.7256	1696.6909	1697.0075	1697.0156
2015.06.08 / 11:34:10	1696.7352	1696.7080	1697.0075	1697.0171
2015.06.08 / 11:34:14	1696.7418	1696.7084	1697.0120	1697.0171
2015.06.08 / 11:34:18	1696.7382	1696.7091	1697.0075	1697.0173
2015.06.08 / 11:34:22	1696.7345	1696.7145	1697.0075	1697.0197
2015.06.08 / 11:34:27	1696.7460	1696.7145	1697.0075	1697.0197
2015.06.08 / 11:38:32	1696.7389	1696.7090	1697.0075	1697.0170
2015.06.08 / 11:38:37	1696.7281	1696.7114	1697.0075	1697.0178
2015.06.08 / 11:38:41	1696.7490	1696.7089	1697.0075	1697.0174
2015.06.08 / 11:38:45	1696.7412	1696.7093	1697.0153	1697.0175
2015.06.08 / 11:38:49	1696.7415	1696.7339	1697.0075	1697.0171
2015.08.04 / 03:18:49	1696.7363	1696.7026	1697.0113	1697.0050
2015.08.04 / 03:21:14	1696.7220	1696.7289	1697.0113	1697.0060
2015.08.04 / 03:27:46	1696.7838	1696.9212	1696.9998	1697.0059
2015.08.04 / 03:28:02	1696.8063	1696.9249	1697.0133	1697.0064
2015.08.04 / 03:28:38	1696.8063	1696.9218	1697.0113	1697.0055
2015.08.20 / 02:25:10	1696.7303	1696.7004	1697.0175	1697.0116
2015.08.20 / 02:28:01	1696.7370	1696.6986	1697.0081	1697.0119

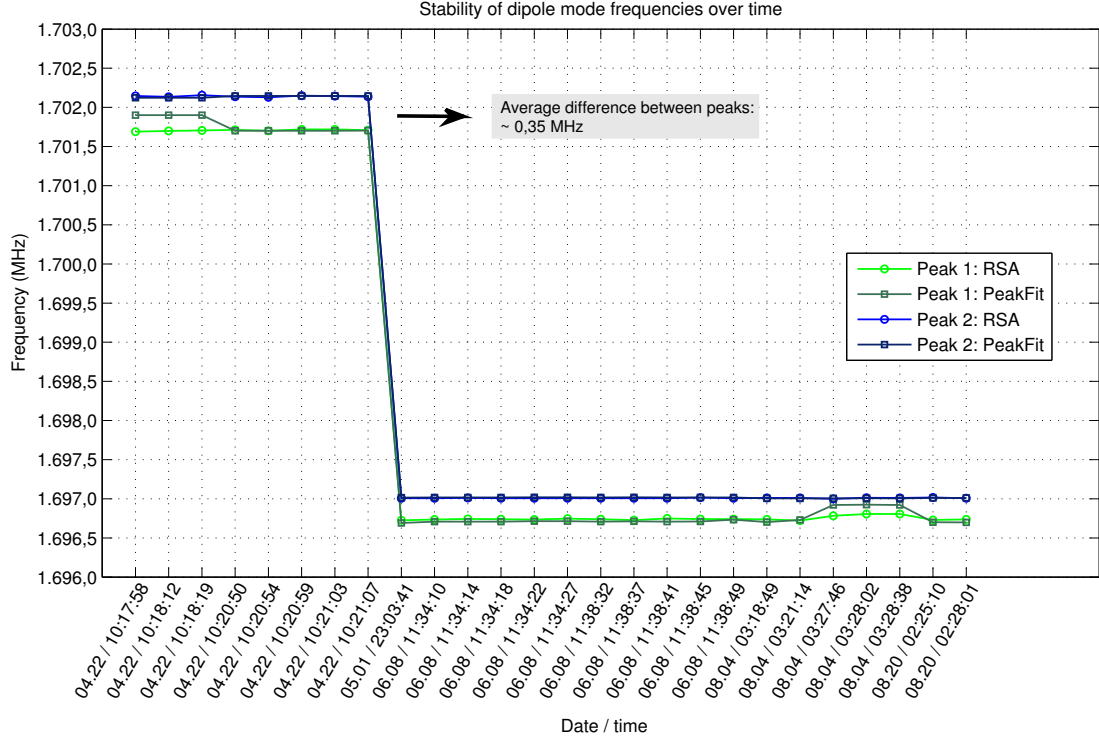


Figure 15: Measured (RSA) and fitted (PeakFit) frequencies of the 2 peaks in the 1st dipole passband for different dates and times.

One can notice a jump of $\sim 5\text{ MHz}$ from the measurements 2015.04.22 to 2015.05.01. This jump in the frequencies is considerable, and will be further studied in Subsection 4.5.

The stability of the measurements before and after the jump are shown in Tables 6 and 7:

Table 6: Average frequencies, standard deviation and relative error of the 2 peaks in the 1st dipole passband for measurements taken on 2015.04.22, before the jump.

Peak	Average frequency (MHz)	Standard deviation (MHz)	Relative error
1	1701.7765	0.1032	0.006%
2	1702.1374	0.0117	0.0007%

Table 7: Average frequencies, standard deviation and relative error of the 2 peaks in the 1st dipole passband for measurements taken from 2015.05.01 onwards, after the jump.

Peak	Average frequency (MHz)	Standard deviation (MHz)	Relative error
1	1696.7486	0.0835	0.005%
2	1697.0136	0.0054	0.0003%

Before and after the frequency shift, the dipole modes of the 1st passband are stable over time.

4.4 Quality Factors

The parameters obtained from the fitting of the peaks from the measured spectra were used to calculate the quality factors for each mode for the different dates and times of measurements.

For the 2nd monopole passband, the results are shown in Table 8 and Figure 16:

Table 8: Calculated quality factors for the 2nd monopole passband on different dates and times.

Date / Time	Peak 1		Peak 2	
	Frequency PeakFit	Quality factor	Frequency PeakFit	Quality factor
2015.08.03 / 22:59:09	2439.1338	5.6×10^4	2449.7356	5.8×10^4
2015.08.03 / 23:57:56	2439.1331	5.6×10^4	2449.7369	5.5×10^4
2015.08.04 / 00:38:20	2439.1339	5.5×10^4	2449.7369	5.4×10^4
2015.08.04 / 00:40:49	2439.1339	4.5×10^4	2449.7371	5.3×10^4
2015.08.04 / 01:44:49	2439.1331	5.3×10^4	2449.7370	5.5×10^4
2015.08.04 / 01:46:21	2439.1309	5.0×10^4	2449.7368	5.3×10^4
2015.08.04 / 01:47:09	2439.1353	5.5×10^4	2449.7369	5.5×10^4
2015.08.04 / 02:12:31	2439.1342	5.3×10^4	2449.7371	5.6×10^4
2015.08.04 / 02:12:49	2439.1341	5.4×10^4	2449.7368	5.5×10^4
2015.08.04 / 02:34:51	2439.1324	5.3×10^4	2449.7367	5.2×10^4
2015.08.04 / 02:38:02	2439.1341	5.5×10^4	2449.7371	5.5×10^4
2015.08.04 / 02:40:52	2439.1317	2.6×10^4	2449.7379	5.3×10^4
2015.08.04 / 03:10:32	2439.1332	5.6×10^4	2449.7372	5.6×10^4
2015.08.04 / 03:11:35	2439.1337	5.4×10^4	2449.7369	5.6×10^4
2015.08.04 / 03:12:02	2439.1336	5.5×10^4	2449.7371	5.6×10^4
2015.08.04 / 03:12:42	2439.1336	5.5×10^4	2449.7371	5.6×10^4
2015.08.04 / 03:29:15	2439.1338	5.6×10^4	2449.7368	5.5×10^4

Date / Time	Peak 3		Peak 4	
	Frequency PeakFit	Quality factor	Frequency PeakFit	Quality factor
2015.08.03 / 22:59:09	2456.9673	1.2×10^5	2462.8447	2.9×10^5
2015.08.03 / 23:57:56	2456.9673	1.2×10^5	2462.8446	2.9×10^5
2015.08.04 / 00:38:20	2456.9673	1.2×10^5	2462.8446	2.8×10^5
2015.08.04 / 00:40:49	2456.9673	1.2×10^5	2462.8445	2.9×10^5
2015.08.04 / 01:44:49	2456.9674	1.2×10^5	2462.8449	2.9×10^5
2015.08.04 / 01:46:21	2456.7897	1.1×10^5	2462.8449	2.9×10^5
2015.08.04 / 01:47:09	2456.9674	1.2×10^5	2462.8447	2.9×10^5
2015.08.04 / 02:12:31	2456.9026	1.2×10^5	2462.8446	2.9×10^5
2015.08.04 / 02:12:49	2456.9671	1.2×10^5	2462.8447	2.9×10^5
2015.08.04 / 02:34:51	2456.9673	1.1×10^5	2462.8446	2.8×10^5
2015.08.04 / 02:38:02	2456.9673	1.2×10^5	2462.8448	2.9×10^5
2015.08.04 / 02:40:52	2456.9673	1.1×10^5	2462.8447	2.8×10^5
2015.08.04 / 03:10:32	2456.9673	1.2×10^5	2462.8446	2.9×10^5
2015.08.04 / 03:11:35	2456.9672	1.2×10^5	2462.8446	2.9×10^5
2015.08.04 / 03:12:02	2456.9673	1.1×10^5	2462.8454	2.4×10^5
2015.08.04 / 03:12:42	2456.9673	1.2×10^5	2462.8447	2.9×10^5
2015.08.04 / 03:29:15	2456.9673	1.2×10^5	2462.8447	2.9×10^5

The fluctuations of the quality factors over time for the 2nd monopole passband are shown in Table 9:

Table 9: Average quality factors, standard deviation and relative error for the 4 peaks of the 2st monopole passband.

Peak	Average Q	Standard deviation	Relative error
1	5.3×10^4	7.5×10^3	14.3%
2	5.5×10^4	1.5×10^3	2.7%
3	1.2×10^5	2.9×10^3	2.5%
4	2.9×10^5	1.3×10^4	4.5%

We can see that the fluctuations of the quality factors for the 2nd monopole passband are of the order of 14% for Peak 1 and $\sim 2 - 4\%$ for Peak 2, Peak 3 and Peak 4.

For the 1st dipole passband, the results for the quality factors for the different dates and times of measurement are shown in Table 10 and Figure 16:

Table 10: Calculated quality factors for the 1st dipole passband on different dates and times.

Date / Time	Peak 1		Peak 2	
	Frequency PeakFit	Quality factor	Frequency PeakFit	Quality factor
2015.04.22 / 10:17:58	1701.9008	6.2×10^4	1702.1238	4.6×10^4
2015.04.22 / 10:18:12	1701.9011	6.0×10^4	1702.1225	4.6×10^4
2015.04.22 / 10:18:19	1701.9015	5.7×10^4	1702.1235	4.5×10^4
2015.04.22 / 10:20:50	1701.7020	3.1×10^4	1702.1460	2.4×10^4
2015.04.22 / 10:20:54	1701.7008	2.9×10^4	1702.1458	2.3×10^4
2015.04.22 / 10:20:59	1701.7016	2.9×10^4	1702.1460	2.3×10^4
2015.04.22 / 10:21:03	1701.7016	3.2×10^4	1702.1460	2.4×10^4
2015.04.22 / 10:21:07	1701.7026	1.5×10^5	1702.1457	1.1×10^5
2015.05.01 / 23:03:41	1701.7765	2.4×10^4	1697.0156	2.0×10^4
2015.06.08 / 11:34:10	1696.7080	3.0×10^4	1697.0171	2.3×10^4
2015.06.08 / 11:34:14	1696.7084	3.6×10^4	1697.0171	1.9×10^4
2015.06.08 / 11:34:18	1696.7091	4.0×10^4	1697.0173	2.0×10^4
2015.06.08 / 11:34:22	1696.7145	3.1×10^4	1697.0197	1.9×10^4
2015.06.08 / 11:34:27	1696.7145	2.7×10^4	1697.0197	1.9×10^4
2015.06.08 / 11:38:32	1696.7090	2.9×10^4	1697.0170	2.0×10^4
2015.06.08 / 11:38:37	1696.7114	2.7×10^4	1697.0178	2.0×10^4
2015.06.08 / 11:38:41	1696.7089	2.9×10^4	1697.0174	2.0×10^4
2015.06.08 / 11:38:45	1696.7093	2.8×10^4	1697.0175	2.0×10^4
2015.06.08 / 11:38:49	1696.7339	4.5×10^4	1697.0171	4.5×10^4
2015.08.04 / 03:18:49	1696.7026	4.4×10^4	1697.0050	4.4×10^4
2015.08.04 / 03:21:14	1696.7289	1.5×10^5	1697.0060	9.0×10^4
2015.08.04 / 03:27:46	1696.9212	1.3×10^5	1697.0059	1.0×10^5
2015.08.04 / 03:28:02	1696.9249	6.4×10^4	1697.0064	1.1×10^5

The fluctuations of the quality factors over time are for the 1st dipole passband are shown in Table 11:

Table 11: Average quality factors, standard deviation and relative error for the 2 peaks of the 1st dipole passband.

Peak	Average Q	Standard deviation	Relative error
1	5.2×10^4	3.8×10^4	75.1%
2	4.1×10^4	3.1×10^4	77.7%

We can see that the fluctuations of the quality factors for Peak 1 and Peak 2 are of the order of $\sim 75\%$. This fluctuation in the values is considerable and should be further studied, being one possible reason the errors in the fitting and the overlapping of modes.

The results of the quality factors over time for both the 2nd monopole passband and the 1st dipole passband are shown in Figure 16:

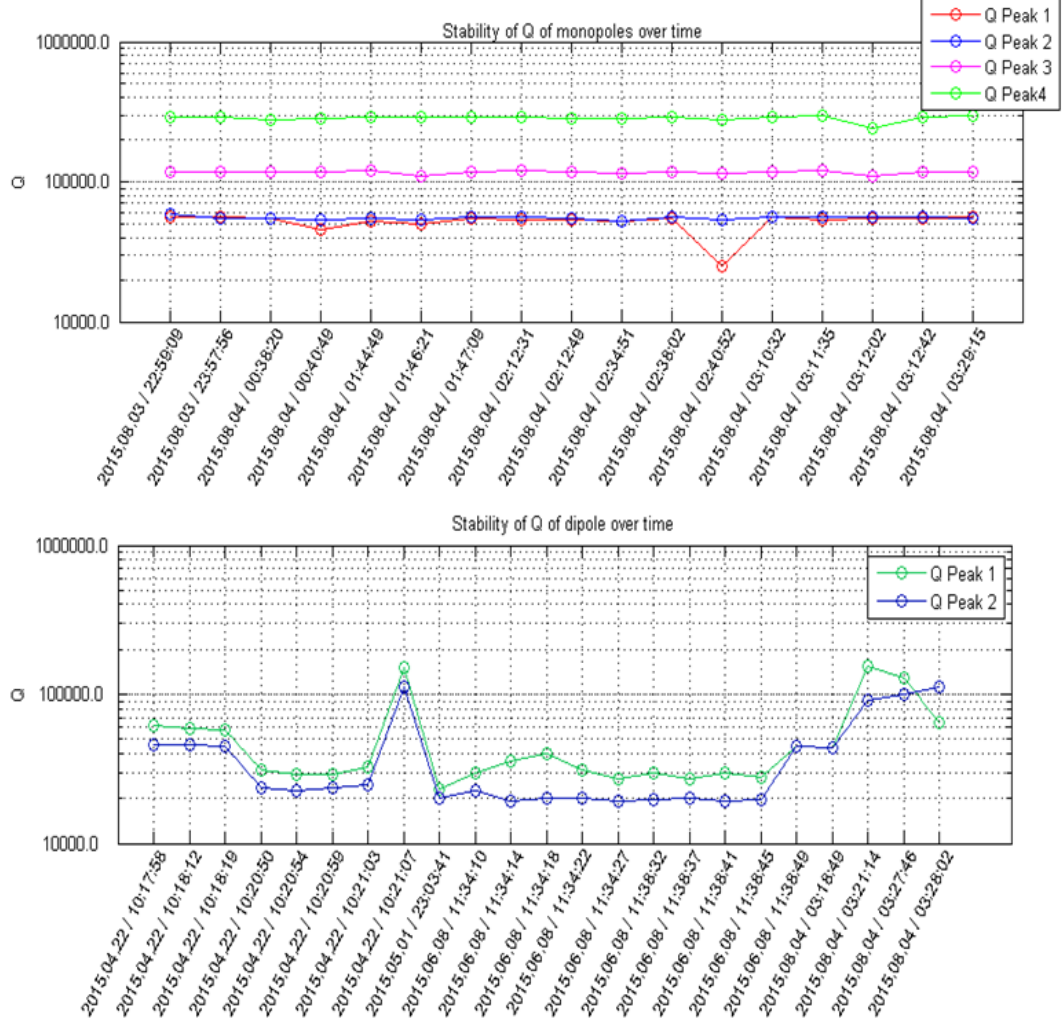


Figure 16: Stability of Q over time for 2nd monopole passband and 1st dipole passband.

4.5 HOM Dependence on the RF Power Applied

It has been considered that a possible reason for the shift observed in the frequency levels of the dipoles (see Subsection 4.3) is the different RF power applied to the cavity while conducting the measurements. Therefore, studies on the influence of the voltage applied on the HOMs were undertaken.

The voltage applied to the 16 cavities in modules ACC6 and ACC7 was gradually increased from 0 MV to 300 MV. Assuming an equal distribution of voltage, the voltage at each cavity varied from 0 MV to 18.750 MV.

The results for the dependence of the 2nd monopole passband are shown in Table 12 and Figure 17:

Table 12: Dependence of the 4 peaks of the 2nd monopole passband with the voltage applied to the cavity.

Voltage (MV)	Frequency Peak 1 (MHz)		Frequency Peak 2 (MHz)	
	RSA	PeakFit	RSA	PeakFit
0.000	2439.1317	2439.0798	2449.7385	2449.7356
1.250	2439.1288	2439.0798	2449.7356	2449.7356
2.500	2439.1317	2439.0798	2449.7327	2449.7356
3.750	2439.1260	2439.0885	2449.7385	2449.7356
5.000	2439.1346	2439.0885	2449.7413	2449.7385
6.250	2439.1375	2439.0856	2449.7385	2449.7385
9.375	2439.1231	2439.0798	2449.7385	2449.7356
12.500	2439.1317	2439.0913	2449.7385	2449.7385
15.625	2439.1317	2439.0913	2449.7356	2449.7356
16.875	2439.1346	2439.0856	2449.7327	2449.7356
18.750	2439.1375	2439.0885	2449.7385	2449.7385

Voltage (MV)	Frequency Peak 3 (MHz)		Frequency Peak 4 (MHz)	
	RSA	PeakFit	RSA	PeakFit
0.000	2456.9673	2456.9673	2462.8462	2462.8462
1.250	2456.9673	2456.9673	2462.8433	2462.8451
2.500	2456.9673	2456.9702	2462.8433	2462.8454
3.750	2456.9702	2456.9673	2462.8462	2462.8453
5.000	2456.9673	2456.9702	2462.8433	2462.8450
6.250	2456.9673	2456.9673	2462.8462	2462.8452
9.375	2456.9673	2456.9673	2462.8462	2462.8454
12.500	2456.9673	2456.9673	2462.8462	2462.8448
15.625	2456.9673	2456.9644	2462.8462	2462.8446
16.875	2456.9673	2456.9702	2462.8433	2462.8448
18.750	2456.9673	2456.9702	2462.8433	2462.8452

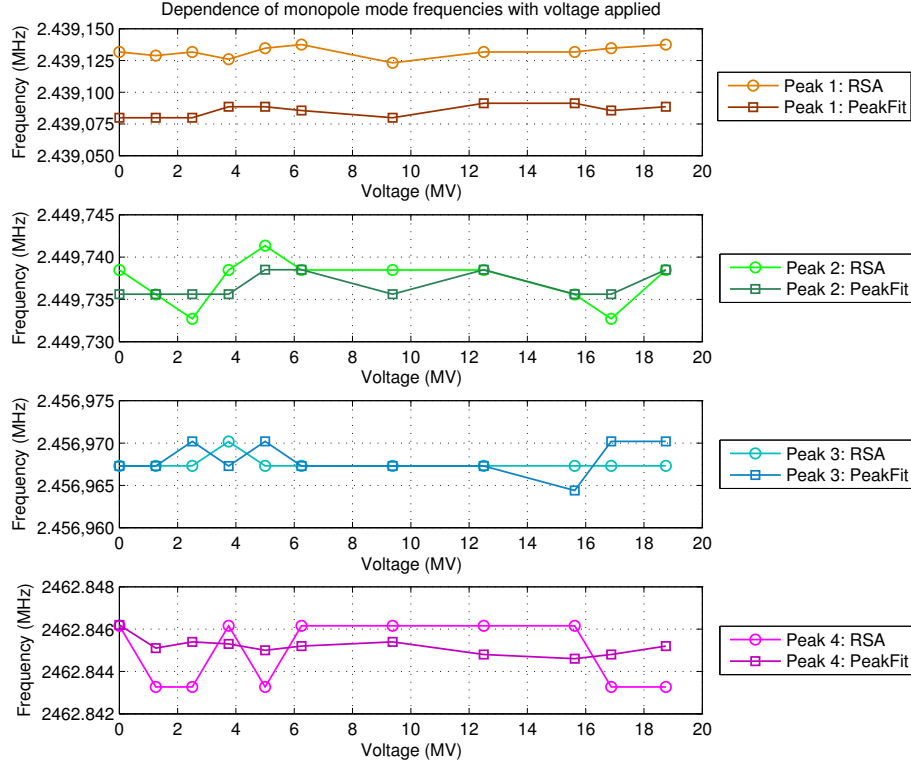


Figure 17: Dependence of the 4 peaks of the 2nd monopole passband with the voltage applied to the cavity.

We can see that the HOMs in this passband are not affected by the voltage applied to the cavity. The fluctuations of each peak while the voltage was increased are shown in Table 13:

Table 13: Average frequencies, standard deviation and relative error of the 4 peaks in the 2nd monopole passband while increasing the voltage applied to the cavity.

Peak	Average frequency (MHz)	Standard deviation (MHz)	Relative error
1	2439.0853	0.0047	0.0002%
2	2449.7367	0.0015	0.00006%
3	2456.9681	0.0019	0.00008%
4	2462.8452	0.0004	0.00002%

One can conclude that the peak frequencies are not affected by the voltage applied to the cavity.

The results for the dependence of the 1st dipole passband with the voltage applied are shown in Table 14 and Figure 18:

Table 14: Dependence of the 2 peaks of the 1st dipole passband with the voltage applied to the cavity.

Power (MV)	Frequency Peak 1 (MHz)		Frequency Peak 2 (MHz)	
	RSA	PeakFit	RSA	PeakFit
0.000	1696.7303	1696.7004	1697.0175	1697.0116
1.250	1696.7494	1696.7232	1697.0175	1697.0040
2.500	1696.7213	1696.6817	1697.0081	1697.0083
3.750	1696.7269	1696.7232	1697.0175	1697.0121
5.000	1696.7254	1696.7121	1696.9961	1697.0059
6.250	1696.7359	1696.7232	1696.9999	1697.0044
9.375	1696.7149	1696.6919	1697.0175	1697.0082
12.500	1696.7479	1696.7404	1696.9999	1697.0055
15.625	1696.7220	1696.7268	1697.0141	1697.0062
16.875	1696.6943	1696.7342	1697.0108	1697.0055
18.750	1696.7201	1696.7195	1696.9999	1697.0059

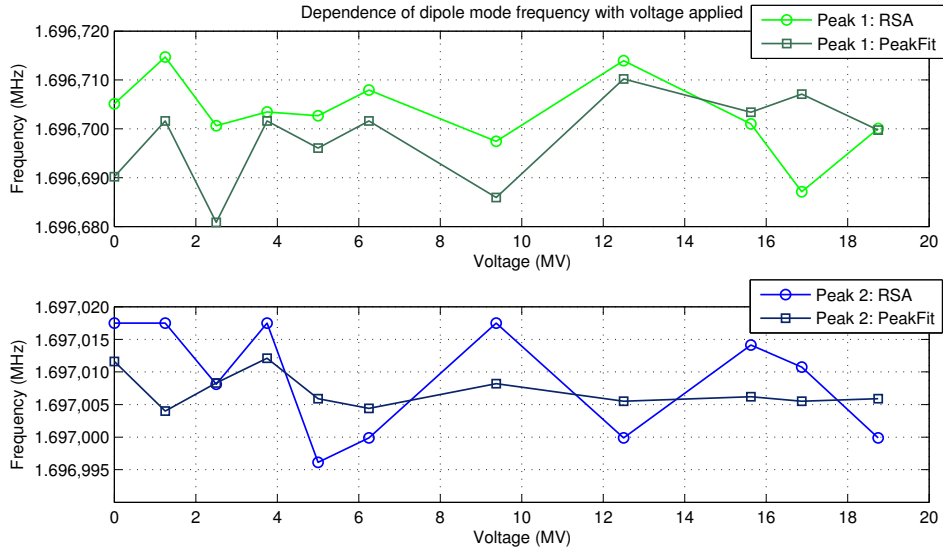


Figure 18: Dependence of the 2 peaks of the 1st dipole passband with the voltage applied to the cavity.

We can see that the HOMs in this passband are not affected by the voltage applied to the cavity. The fluctuations of each peak while the voltage was increased are shown in Table 15:

Table 15: Average frequencies, standard deviation and relative error of the 2 peaks in the 1st dipole passband while increasing the voltage applied to the cavity.

Peak	Average frequency (MHz)	Standard deviation (MHz)	Relative error
1	1696.7161	0.0180	0.001%
2	1697.0070	0.0027	0.0002%

One can conclude that the peak frequencies are not affected by the voltage applied to the cavity. Therefore, a further study should be conducted in order to understand the jump of the dipole frequencies in time that was previously described in Subsection 4.3.

5 S-parameter Measurements in Third Harmonic Cavities for the E-XFEL

In the Third Harmonic Superconducting Cavities at the E-XFEL, it is envisioned to make use of HOMs for beam diagnostics as well. The aim is to provide beam position information from the energy radiated to the HOM couplers. In order to use the HOMs from the coupled cavities as BPM, it is essential to characterize the HOMs in each of the 8 cavities and understand their behavior.

In order to understand the spectrum of the 8 coupled cavities in the , it is important to know the spectrum of each individual cavity. Accordingly, we used Vector Network Analyzer to measure the transmission spectra of the cavities. The modes were then identified using a global Lorentzian fit technique.

5.1 Measurement of S_{21} Parameter with NWA

Measurements were undertaken for single cavities. Inside the single cavities there was vacuum at room temperature. Cavity 3HZ010 was measured in the warm and the superconducting environments, while the others were measured only at room temperature.

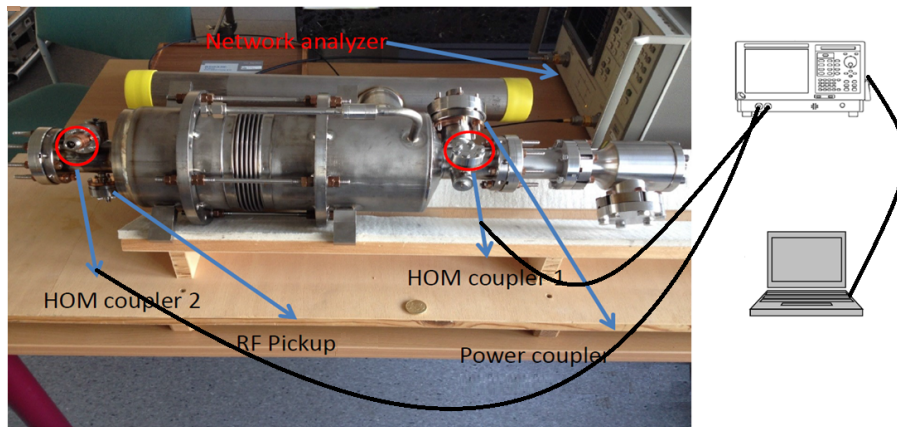


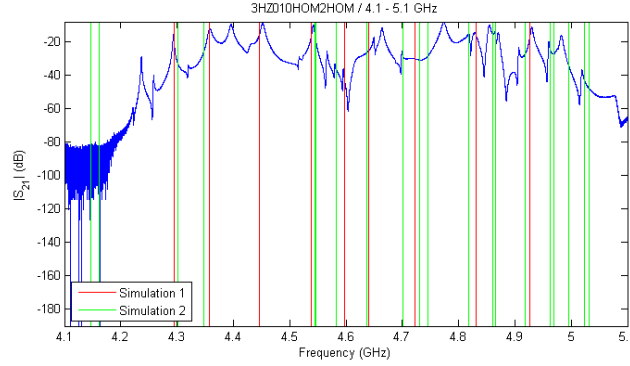
Figure 19: Single cavity RF transmission measurement.

The transmission measurements were conducted by using a VNA (HP8720C), a laptop, a GPIB to USB adapter and RF cables. Refer to the Figure 19

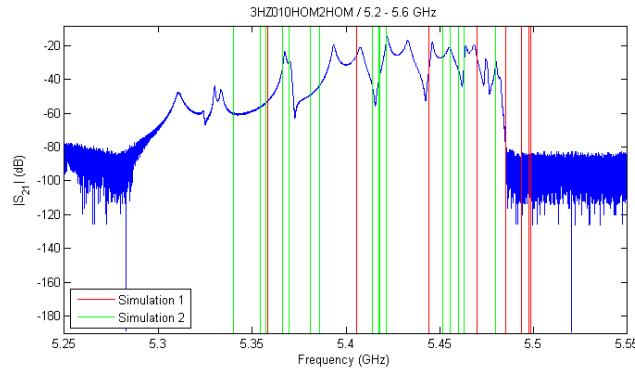
The VNA, injected a wide frequency spectrum signal from the HOM coupler 1, and measured the transmitted signal to the HOM coupler 2. This way, one obtains the S_{21} parameter of the cavity. The transmission spectrum (S_{21}) was subsequently measured for each single cavity. The measurements were focused on the cavity modes in the first two dipole bands (4-5.6 GHz) and in the fifth dipole band (9-9.1 GHz).

5.2 Transmission Spectra and HOM Characterization for Single Cavities at Room Temperature

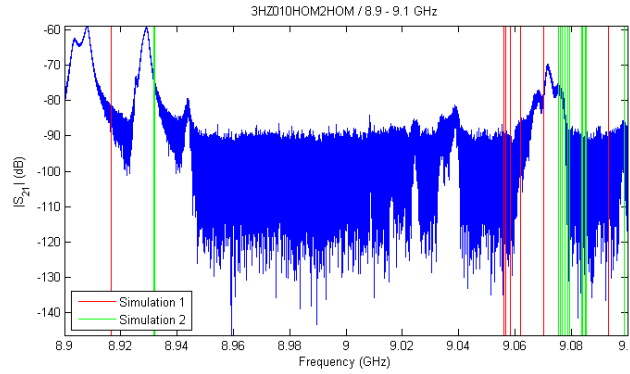
The HOM signals measured from the all eight cavities can be found in Appendix A.



(a) The first dipole band



(b) The second dipole band



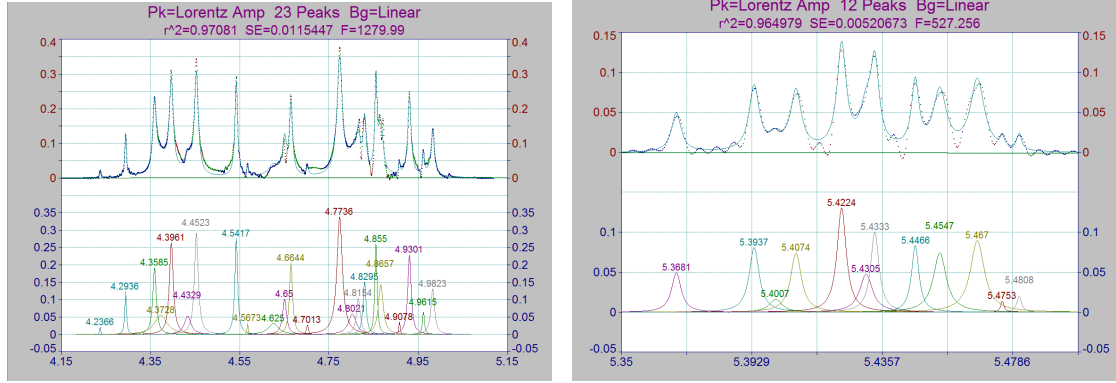
(c) The fifth dipole band

Figure 20: Typical transmission spectrum (S_{21}) of the isolated cavity 3HZ010. The vertical lines indicate simulation results of the modes. The colors red and green represent simulation 1 [3] and simulation 2 [4] respectively.

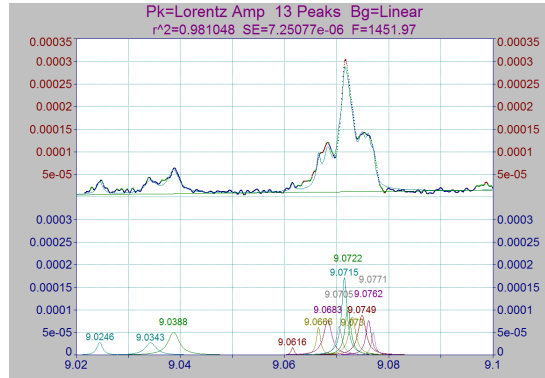
A typical transmission spectrum is shown in Figure 20 along with simulations. The simulations are performed on an ideal single cavity without couplers[3] (simulation 1) and with couplers[4] (simulation 2). Specific regions are respectively the first two dipole bands (Figure 20(a) 20(b)) and the fifth dipole band (Figure 20(c)).

The couplers breaks the symmetry of the structure. This accounts for differences between simulations and measurements. In addition, other sources such as fabrication errors and cavity tuning can also contribute to the differences to the simulations. However the comparison with simulation helps us identify many of the modes.

Each peak of the spectrum was fitted with PeakFit as a Lorentzian distribution. The results of such fit for cavity 3HZ010 are shown in Figure 21



(a) The first dipole band, up: measured; down: the outcome of the fit. The numbers show the peak center frequencies. The coefficient of determination r^2 is shown above the plots.



(c) The fifth dipole band, up: measured; down: the outcome of the fit. The numbers show the peak center frequencies. The coefficient of determination r^2 is shown above the plots.

Figure 21: Fit of the first two dipole bands and the fifth dipole band of cavity 3HZ010 as Lorentzian distributions.

Lorentzian fit of the single cavity data from 3HZ010HOM2HOM					
Measurement		Simulation			
freq(GHz)	Q	Electric boundary		Magnetic boundary	
		f(GHz) EE	Q EE	f(GHz) MM	Q MM
4.2365	1.56E+03	4.1609	551000	4.1462	386000
4.2935	9.66E+02	4.3014	2000	4.3474	1500
4.3585	4.72E+02	4.5445	1860	4.5462	1240
4.3727	1.29E+02	4.582	740	4.731	200
4.3961	4.22E+02	4.637	1640	4.866	1630
4.4328	2.46E+02	4.7015	850	4.9686	16100
4.4522	4.37E+02	4.7449	2270	4.9696	11900
4.5417	6.16E+02	4.8174	555	5.0234	25600
4.5672	1.71E+03	4.8603	1460	5.0242	84300
4.625	1.64E+02	4.9175	386		
4.65	4.41E+02	4.962	1180		
4.6644	5.68E+02	4.996	400		
4.7013	8.93E+02	5.0317	6510		
4.7735	3.30E+02				
4.8021	2.27E+02				
4.8154	4.69E+02				
4.8294	6.03E+02				
4.8549	8.59E+02				
4.8657	3.76E+02				
4.9077	1.59E+03				
4.9301	5.45E+02				
4.9615	9.68E+02				
4.9823	5.01E+02				

Table 16: Peaks in the first dipole band in Figure 21(a)

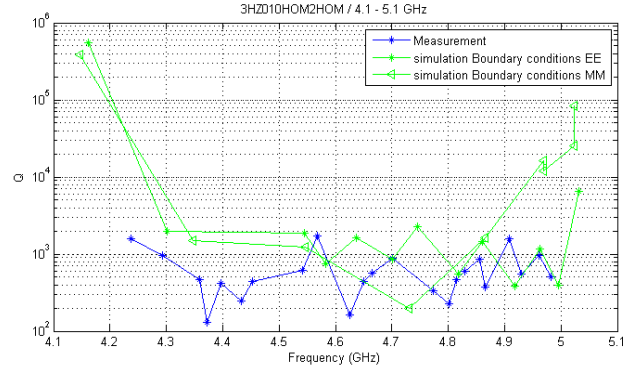
Lorentzian fit of the single cavity data from 3HZ010HOM2HOM					
Measurement		Simulation			
freq(GHz)	Q	Electric boundary		Magnetic boundary	
		f(GHz) EE	Q EE	f(GHz) MM	Q MM
5.3681	1.41E+03	5.3400	1.00E+03	5.3544	2.45E+05
5.3936	1.35E+03	5.3664	6.22E+03	5.3573	1.85E+03
5.4007	1.04E+03	5.3695	8.00E+02	5.3810	4.08E+04
5.4074	1.27E+03	5.4181	6.37E+03	5.3860	5.00E+02
5.4224	1.48E+03	5.4215	1.02E+03	5.4143	3.63E+03
5.4304	1.07E+03	5.4599	9.35E+03	5.4176	5.26E+04
5.4333	1.63E+03	5.4630	1.10E+03	5.4516	2.37E+04
5.4466	1.84E+03			5.4556	3.58E+04
5.4546	1.05E+03			5.4797	1.76E+04
5.4670	9.88E+02			5.4834	3.72E+04
5.4752	4.09E+03				
5.4808	2.85E+03				

Table 17: Peaks in the second dipole band in Figure 21(b).

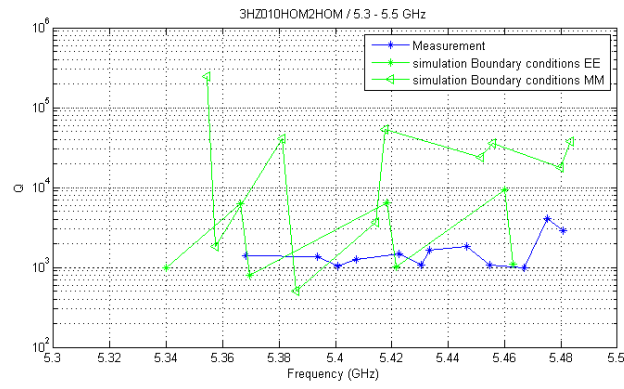
Lorentzian fit of the single cavity data from 3HZ010HOM2HOM					
Measurement		Simulation			
freq(GHz)	Q	Electric boundary		Magnetic boundary	
		freq(GHz)	Q	freq(GHz)	Q
9.0245	6.85E+03	9.0756	708000	9.0756	10600000
9.0343	3.62E+03	9.0761	295000	9.0761	3870000
9.0387	3.52E+03	9.0796	295000	9.0763	175000000
9.061	1.34E+04	9.0839	44000	9.0768	3530000
9.0665	9.79E+03	9.0853	146000	9.0778	8380000
9.0683	4.89E+03	9.1009	85900	9.0787	2110000
9.0705	6.90E+03			9.0795	5900000
9.0715	7.30E+03			9.0837	758000
9.0721	7.08E+03			9.0851	1540000
9.0730	5.66E+03			9.0989	170000
9.0748	5.07E+03			9.1006	188000
9.0761	7.30E+03				
9.0770	1.06E+04				

Table 18: Peaks in the fifth dipole band in Figure 21(c)

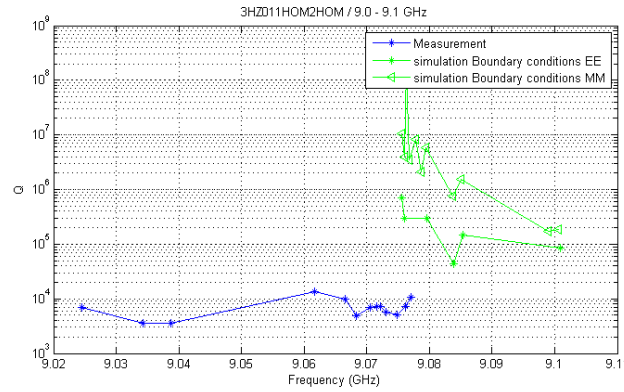
The quality factors obtained for each mode are compared with the simulation 2 [4] in Figure 22



(a) The first dipole band



(b) The second dipole band



(c) The fifth dipole band

Figure 22: Measured and simulated Q for the warm single cavity 3HZ010.

The Q factors from the measurement are lower than the results of simulation. This is expected, due to the higher losses at room temperature.

Figure 23 shows that the HOMs from each of the eight cavities.

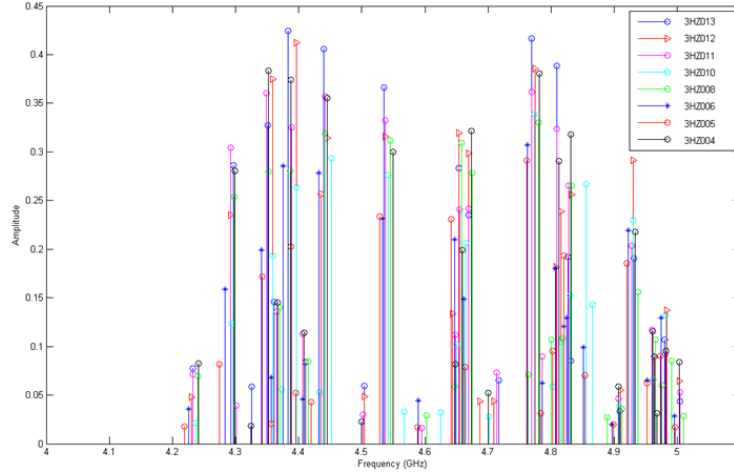
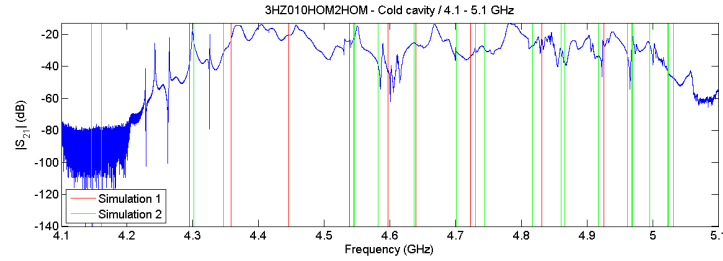


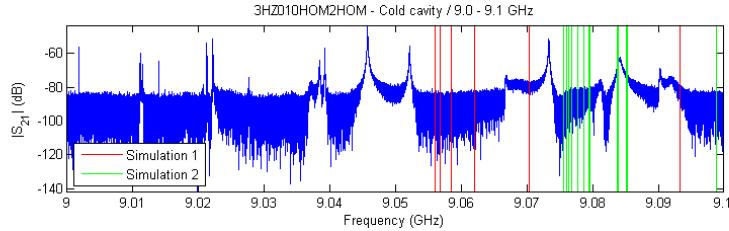
Figure 23: HOMs from eight cavities

Each line represents a mode obtained by fitting. The HOMs from each of the eight cavities basically remain close to each other. This reflects that the geometry of the eight cavities is also similar to each other.

5.3 Transmission Spectra and HOM Characterization for a Single Cold Cavity



(a) The first dipole band



(b) The fifth dipole band

Figure 24: Typical transmission spectrum (S_{21}) of the isolated cavity 3HZ010 in superconducting condition. The vertical lines indicate simulation results of the modes. The colors red and green represent simulation 1 [3] and simulation 2 [4] respectively.

Lorentzian fit of the single cavity data from 3HZ010HOM2HOM(cold)					
Measurement		Simulation			
		Electric boundary		Magnetic boundary	
freq(GHz)	Q	f(GHz) EE	Q EE	f(GHz) MM	Q MM
4.3001	9.60E+02	4.1609	551000	4.1462	386000
4.3688	2.74E+02	4.3014	2000	4.3474	1500
4.4033	2.64E+02	4.5445	1860	4.5462	1240
4.4213	3.06E+02	4.582	740	4.73	200
4.4443	3.99E+02	4.637	1640	4.866	1630
4.4572	6.14E+02	4.7015	850	4.9686	16100
4.4664	1.68E+02	4.7449	2270	4.9696	11900
4.5194	5.84E+02	4.8174	555	5.0234	25600
4.5353	2.89E+02	4.8603	1460	5.0242	84300
4.5505	6.91E+02	4.9175	386		
4.5898	1.20E+03	4.962	1180		
4.6367	2.15E+02	4.996	400		
4.6686	4.79E+02	5.0317	6510		
4.6856	2.03E+02				
4.7384	2.61E+02				
4.7828	4.14E+02				
4.7938	2.08E+02				
4.8248	6.82E+02				
4.8386	5.08E+02				
4.8605	2.19E+03				
4.8796	4.69E+02				
4.9008	4.49E+02				
4.9391	3.25E+02				
4.9514	4.62E+02				
4.9699	1.79E+03				

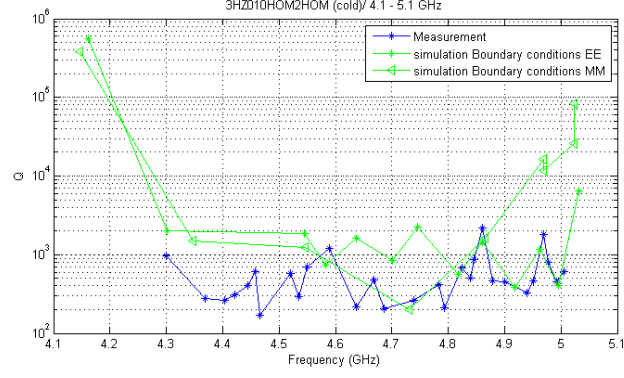
Table 19: Table of peaks in Figure 25(a)

Lorentzian fit of the single cavity data from 3HZ010HOM2HOM					
Measurement		Simulation			
		Electric boundary		Magnetic boundary	
freq(GHz)	Q	f(GHz) EE	Q EE	f(GHz) MM	Q MM
5.3216	2.11E+03	5.3400	1.00E+03	5.3544	2.45E+05
5.3305	1.58E+03	5.3664	6.22E+03	5.3573	1.85E+03
5.3364	1.27E+03	5.3695	8.00E+02	5.3810	4.08E+04
5.3908	7.68E+02	5.4181	6.37E+03	5.3860	5.00E+02
5.4214	1.15E+03	5.4215	1.02E+03	5.4143	3.63E+03
5.4300	1.42E+03	5.4599	9.35E+03	5.4176	5.26E+04
5.4374	1.50E+04	5.4630	1.10E+03	5.4516	2.37E+04
5.4531	2.01E+03			5.4556	3.58E+04
5.4651	4.12E+03			5.4797	1.76E+04
5.4729	2.02E+03			5.4834	3.72E+04
5.4820	2.45E+03				
5.4897	1.57E+03				

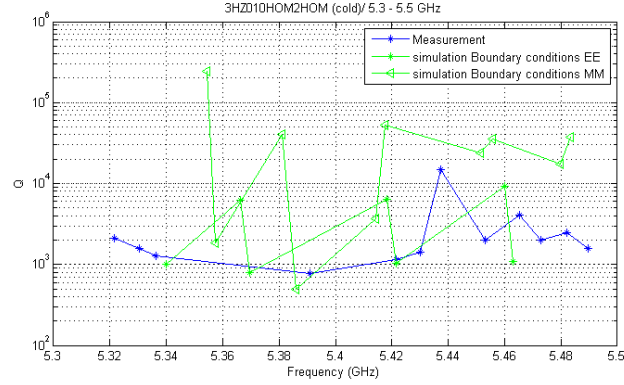
Table 20: Table of peaks in Figure 25(b)

Lorentzian fit of the single cavity data from 3HZ010HOM2HOM					
Measurement		Simulation			
		Electric boundary		Magnetic boundary	
freq(GHz)	Q	f(GHz) EE	Q EE	f(GHz) MM	Q MM
9.0112	2.47E+04	9.0756	708000	9.0756	10600000
9.0222	3.53E+04	9.0761	295000	9.0761	3870000
9.0384	2.97E+04	9.0796	295000	9.0763	175000000
9.0392	3.62E+04	9.0839	44000	9.0768	3530000
9.0457	3.25E+04	9.0853	146000	9.0778	8380000
9.0463	5.78E+04	9.1009	85900	9.0787	2110000
9.0521	3.06E+04			9.0795	5900000
9.0733	2.76E+04			9.0837	758000
9.0812	2.94E+04			9.0851	1540000
9.0842	1.03E+04			9.0989	170000
9.0903	2.67E+04			9.1006	188000
9.0918	6.79E+03				

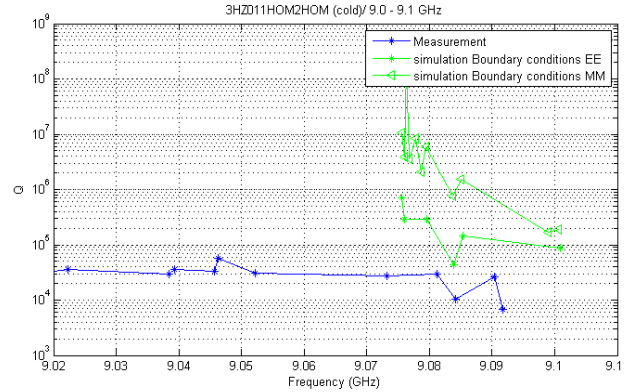
Table 21: Table of peaks in Figure 25(c)



(a) The first dipole band



(b) The second dipole band



(c) The fifth dipole band

Figure 26: The Q obtained from the cold single cavity 3HZ010 and simulation

The Q factor for the cold cavity is higher than that for the warm cavity, but are still lower than simulations.

One should also note that, in the fifth dipole band, the mode frequency from simulation at 9.07-9.09 GHz are quite different from the fitting results. This may be because higher frequencies mean the shorter wavelengths, and therefore the short wavelength influenced easier by geometrical changes.

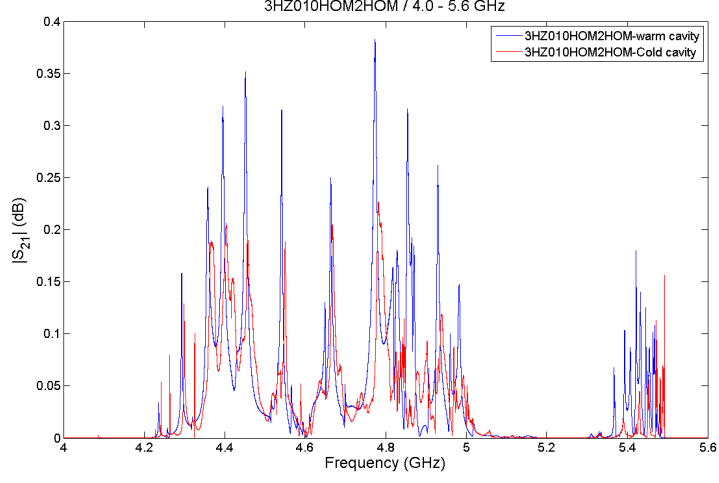


Figure 27: Comparison of the warm and cold s-parameter spectra

Figure 27 shows that the cutoff frequency of the first dipole band measured at home temperature is smaller than which measured in superconducting condition. This is consistent with the theoretical calculations.

6 Conclusions

In the 1.3 GHz cavities case, the HOM measurements were conducted using a Real-time Spectrum Analyzer, that takes the signals from both HOM couplers and records real-time spectra. Considering the impact on some systematic errors due to the noise present in the spectra, HOMs were also identified by using a global Lorentzian fit technique. The parameters resulting from each peak were further used to calculate the Q factor for each mode.

From the results we can conclude that the peak frequencies of the 2nd monopole passband remain constant in time. It is not the case of the 1st dipole passband, where we noticed a considerable frequency shift of the dipole modes from the measurements taken on 2015.05.01 onwards. In the case of the monopole modes, we found deviations in the Q factors of the order of 2-14%. Nonetheless, in the case of the dipole modes, the deviations of the quality factors were of the order of 75%. Regarding the influence of the RF power applied to the cavity and the stability of these spectra, we can conclude that the peak frequencies for both monopole and dipole modes are not affected by the power applied to the cavity. Therefore, a further study should be conducted in order to understand the 5MHz shift of the dipole frequency levels in time.

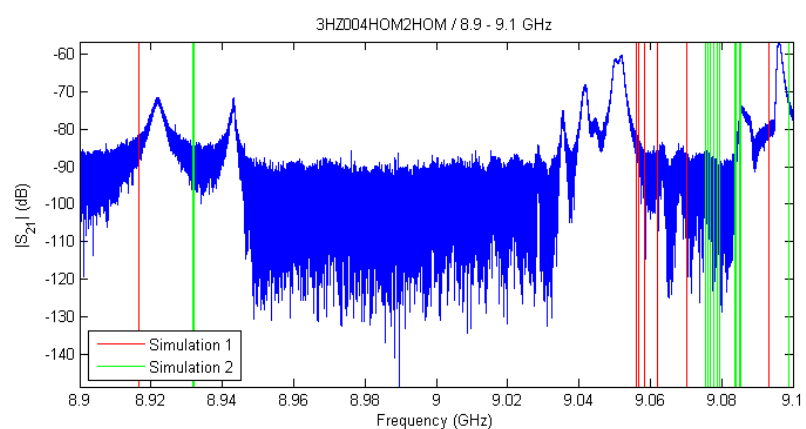
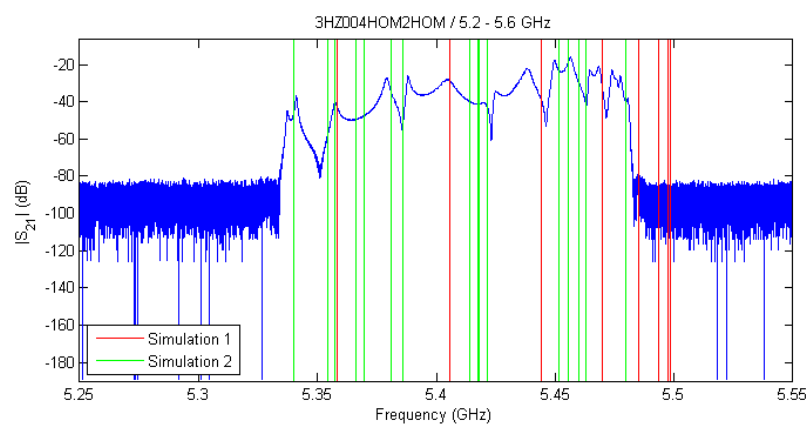
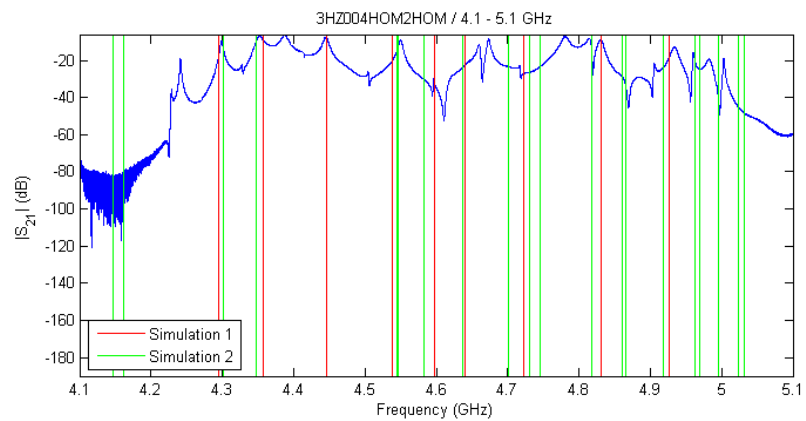
In the 3.9 GHz cavities case, we measured each of the eight single cavities for the E-XFEL at room temperature, while cavity 3HZ010 was also measured in superconducting condition. We obtained the first two dipole bands (4-5.6GHz) and the fifth dipole band (9-9.1 GHz) S-parameter spectrum by using a Vector Network Analyzer. PeakFit was used to identify resonant peaks in the spectrum, and calculate the frequency and the Q factor of each mode. Finally, we compared the fitting results with the simulationS.

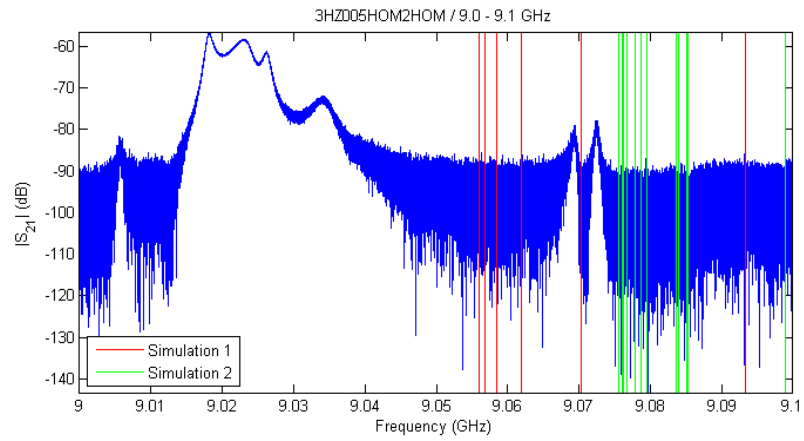
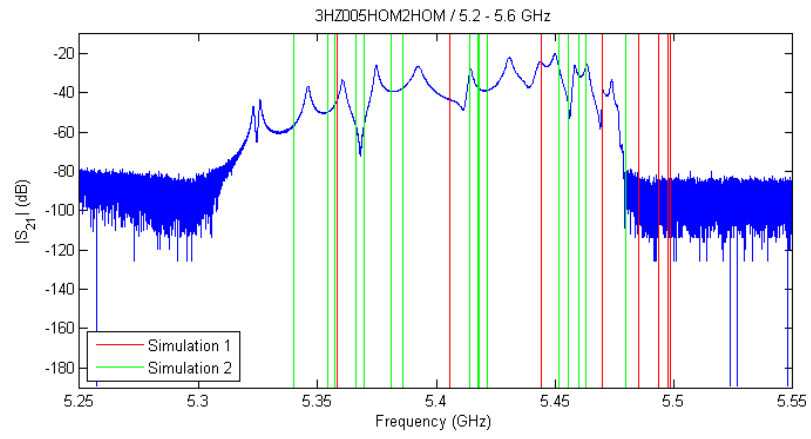
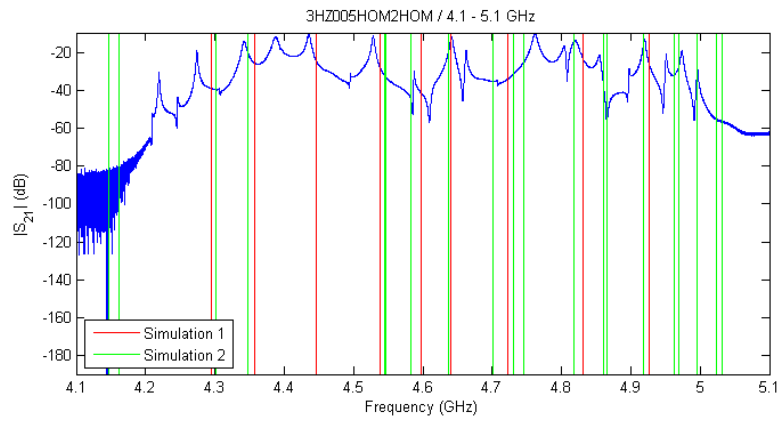
From the analysis we can conclude that the HOMs in each of the eight cavities basically remain close to each other. This reflects that the eight cavities don't have obvious geometrical differences. For the 5th dipole band, the modes are shifted to higher frequencies with respect to the simulation. HOMs at such high frequencies are very sensitive to geometrical changes. For the Q factors we can clearly see a gap between simulation and fit. In superconducting condition, the gap is small, but does not disappear.

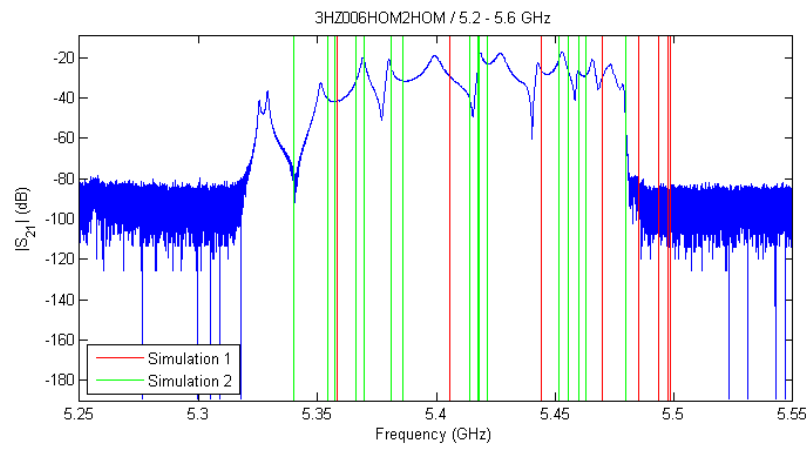
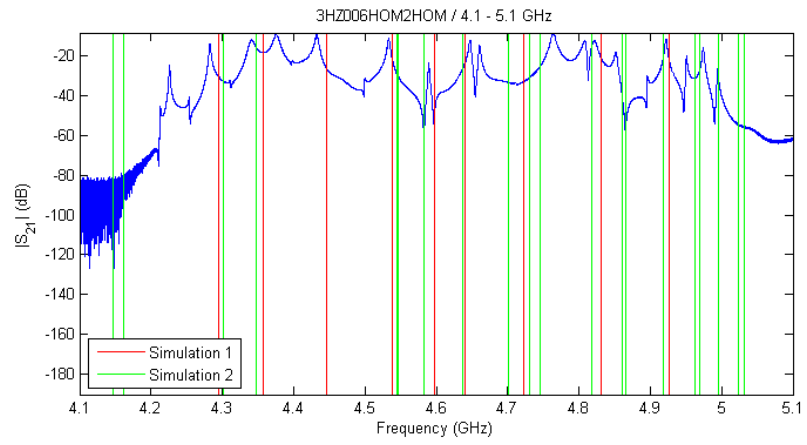
References

- [1] R. Wanzenberg. *Monopole, Dipole and Quadrupole Passbands of the TESLA 9-cell Cavity*. TESLA 2001-33. 2001.
- [2] P. Zhang, N. Baboi, R. M. Jones. *Higher order mode spectra and the dependence of localized dipole modes on the transverse beam position in third harmonic superconducting cavities at FLASH*. DESY 12-109. 2013.
- [3] I. Shinton, N. Juntong. *Compendium of eigenmodes in third harmonic cavities for FLASH and the XFEL*. DESY 12-053. 2012.
- [4] T. Khabibouline, N. Solyak, R. Wanzenberg. *Higher Order Modes of a 3rd Harmonic Cavity with an Increased End-cup Iris*. TESLA-FEL 2003-01. 2003.
- [5] N. Baboi. *Studies on Higher Order Modes in Accelerating Structures for Linear Colliders*. PhD Thesis. Hamburg, 2001.
- [6] A. Fabris, C. Pasotti, P. Pittana, M. Svandrlik. *Design Of a 3rd Harmonic Superconducting Cavity For Bunch Lengthening In ELETTRA*. Proceedings of EPAC98, p.1879-1881, Stockholm, Sweden
- [7] P. Pierini, A. Bosotti, P. Michelato, L. Monaco, R. Paparella, D. Sertore, E. Vogel. *XFEL Third Harmonic Superconducting Cavity Prototypes fabrication and processing experience*. Proceedings of SRF2009, p.844-848, Berlin, Germany.
- [8] P. Pierini, A. Bosotti, N. Panzeri, D. Sertore, H. Edwards, M. Foley, E. Harms, D. Mitchell, J. Iversen, W. Singer, E. Vogel *Third Harmonic Superconducting Cavity Prototypes for the XFEL*. Proceedings of LINAC08, p.821-823, Victoria, BC, Canada.
- [9] flash.desy.de/
- [10] www.xfel.eu/
- [11] www.mathworks.com
- [12] www.sigmaplot.com/products/peakt/peakt.php

7 Appendix: 3.9 GHz Cavities







#

